Materials Advances

ROYAL SOCIETY OF CHEMISTRY

PAPER

View Article Online
View Journal | View Issue

Cite this: *Mater. Adv.*, 2025, **6**, 7056

Colour tuneable luminescent organic–inorganic hybrid materials based on lanthanide-doped ionic liquid polymers†

Olivier Renier, [a] Guillaume Bousrez, [ab] Veronica Paterlini, [a] Magdalena Wilk-Kozubek [ac] and Anja-Verena Mudring [*abd]

Received 28th March 2025,
Accepted 5th August 2025

DOI: 10.1039/d5ma00282f

rsc.li/materials-advances

Highly luminescent organic–inorganic hybrid materials have been prepared by combining task-specific polymerized ionic liquids (PILs) based on the 1-alkyl-3-vinylimidazolium cation ($[C_nVim]^+$ (with n = 2–6)) with suitable halides of trivalent lanthanides such as europium and terbium. The resulting materials have been characterized by ^{1}H nuclear magnetic resonance, Fourier transform infrared, UV-Vis and photoluminescence spectroscopy. They show bright and intense luminescence over a wide range of excitation wavelengths, which particularly for the Eu^{3+} containing compounds, benefits from efficient energy transfer from the organic aromatic moieties in the PIL to the emitting level of the lanthanide(III) ion. In the case of the Tb^{3+} ion, the emission benefits from excitation into the Tb^{3+} d levels. The emission colour can be tuned from green to red for Tb and Eu respectively. This includes bright white emission for Eu that can be achieved by altering the excitation wavelength. The easy processability of these novel PILs renders them interesting for a wide range of optical applications.

Introduction

Reducing energy consumption is increasingly important, if the goals for a sustainable society should be met. Lighting, in particular, constitutes a significant share.[1,2] Although the inefficient incandescent lamps are phased out around the world,[3] and are swapped by more energy efficient lighting technologies, the increased demand for lighting is off-setting energy savings. For improved energy efficiency and lower environmental footprint, the first generation of energy-efficient replacements, the compact fluorescent lamps (CFLs), are now mostly replaced by light-emitting diodes (LEDs). However, these stress the demand for critical raw materials,[4] in particular gallium and indium. OLEDs (organic light emitting diodes) and LECs (light-emitting electrochemical cells) offer a way out of this dilemma. In addition, they bear advantages with respect to architectural features (flexibility and large areal illumination) and manufacturing.[5] Whilst transition metal complexes have been widely studied and applied in these technologies as emitter materials, lanthanide complexes have been investigated far less.[6,7] Yet, with respect to colour-purity, temperature independent emission and oxidation stability they offer advantages hardly attainable from other materials. The reason that lanthanide ions are widely used as the luminescent centres is because of their efficient and well-defined, narrow line emission, resulting from the shielding of the f-electrons by the outer 4d and 5p-levels.[8–10] Their relevance with respect to energy technologies like lighting is one of the reasons for rendering them critical raw materials. Meanwhile mitigation strategies such as recycling, including urban mining and use in low concentration have emerged as successful mitigation strategies, allowing them to be reconsidered for applications.[11] Generally, the highest luminescent quantum yields are obtained for complexes of Tb^{3+} and Eu^{3+} rendering them preferred emitter materials for emission in green and red. To quench the emissive state through OH-vibrations (*e.g.* from ubiquitous water), the third harmonics of the OH-vibration, and for Tb^{3+} the fourth is needed, as the energy difference between the emitting state and the nearest lower-lying state is fairly large.

An interesting prospect for application is the inclusion of lanthanide complexes into a polymer. The main benefits of developing luminescent polymers for application are their durability, flexibility and, most importantly, facile processability, namely spin-coating and solution casting.[12] Classical polymers such as poly-methyl-methacrylate (PMMA) have already been

[a] *Department of Materials and Environmental Chemistry, Stockholm University, Svante Arrhenius väg 16C, 10691 Stockholm, Sweden*
[b] *Department of Biological and Chemical Engineering and iNANO, Aarhus University, Åbogade 40, 8200 Aarhus N, Denmark. E-mail: anja.mudring@rub.de, anja-verena.mudring@bce.au.dk*
[c] *Department of Nanotechnology, PORT Polish Center for Technology Development, 147 Stabłowicka Street, 54-066 Wrocław, Poland*
[d] *Department of Physics, Umeå University, Linnaeus väg 24, 901 87 Umeå, Sweden. E-mail: anja-verena.mudring@umu.se*
† In memory of Georges Boulon

doped with lanthanide complexes such as lanthanide β-diketonates[13,14] and for such materials, it has been observed that often, a narrower and more intense emission occurs when compared to the neat bulk material.[15]

In this context, ionic polymers are yet to be explored as hosts for lanthanide phosphors and may provide interesting features, in particular for applications in light emitting electrochemical cells. Such compounds can be made from ionic liquids (ILs) bearing polymerizable moieties, and are therefore referred to as polymeric or polymerized ionic liquids (PILs).[16–21] On the one hand, ionic polymers based on polymerizable ILs have already been explored as solid electrolytes.[22] On the other hand it has already been shown that ILs, or low-temperature molten salts, can be endowed with luminescent properties by both the inclusion of the lanthanide ion in the form of a complex ion,[23–37] and by the synthesis of lanthanide-containing nanoparticles (NPs) directly in the ILs.[34,38–46] The optical properties of the obtained materials benefited in many cases from the IL properties. A proof-of-concept has been given for luminescent nanoparticles in PILs, where the all-in-one synthesis of luminescent polymer-nanoparticles led to composite materials with good results.[47] Herein, we report the novel approach of endowing PILs with a luminescent active centre in the non-polymeric anion part of the material. For that reason, a set of 1-alkyl-3-vinylimidazolium halide-based PILs was synthesised and doped with europium(III) and terbium(III) halides.

Results and discussion

In order to obtain the lanthanide-based luminescent PILs, first 1-alkyl-3-vinylimidazolium bromide PILs were prepared by quaternization of 1-vinylimidazole with alkylbromides of different chain lengths (C_2–C_6),[48] which were then polymerized *via* free radical polymerization using azo-bis(isobutyro)nitrile (AIBN) in chloroform (Scheme 1).[49,50]

The success of the polymerization reactions could be confirmed by nuclear magnetic resonance (NMR), Fourier Transform Infrared (FTIR) spectroscopy (see Fig. S1–S25) and UV-Vis spectroscopy. The ^{1}H-NMR spectra of the IL monomers (C_nVimBr (n = 2–6)) feature three doublet of doublets signals at around 5.40, 6.03 and 7.35 ppm arising from the vinyl protons. After polymerization, these signals are not found in the ^{1}H-NMR spectra of the corresponding PILs (P-C_nVimBr (n = 2–6)), confirming successful polymerization (see Fig. S11–S14). The ^{1}H-NMR spectra of the respective PILs display very broad signals which in some areas even overlap each other which are caused by the formation of different hydrocarbon backbones during the polymerization process, a feature commonly observed.[51] All of the NMR spectra match the previously for those compounds reported data.[52]

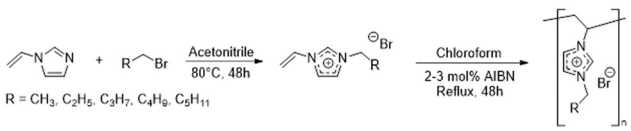

Scheme 1 General synthesis of 1-alkyl-3-vinylimidazolium bromide ILs (C_nVimBr (n = 2–6)) and poly-1-alkyl-3-vinylimidazolium bromide (P-C_nVimBr (n = 2–6)).

The FTIR spectra of IL monomers exhibit two characteristic bands in the regions of 960–985 cm^{-1} and 915–930 cm^{-1} that are assigned to the C–H out-of-plane deformation vibrations of the vinyl group. These bands are also not observed in the FTIR spectra of the corresponding PILs (see Fig. S16–S25). The bands above 3040 cm^{-1} associated with the C–H stretching vibrations of the vinyl group cannot serve as an indicator of polymerization progress because they are overlapped by bands related to the aromatic C–H stretching vibrations.[53]

Differential scanning calorimetry (DSC) was carried out to characterize the thermal behaviour of both, the mono- as well as the polymers (see Fig. S26 and S35). Upon the first heating, C_2VimBr starts to melt at 64.3 °C and during the first cooling the compound recrystallises at 59.1 °C. The second heating shows two transitions with the first one at 87.2 °C directly followed by the second one at 93.7 °C. The second cooling leads to a recrystallisation step at 57.5 °C. The following cycles are reproducible. C_3VimBr and C_6VimBr display similar thermal behaviour as they could not be obtained as a crystalline solid. The first one, after the removal of the moisture during the first heating, only vitrification and devitrification can be observed upon cooling and heating around −40 °C and the second one has its glass transition around −35 °C. Also, both C_4VimBr and C_5VimBr show very similar thermal behaviour. The virgin samples melt at 81.6 °C and 51.8 °C. No crystallization, only glass transitions at −30 °C and −29 °C upon cooling and devitrification on heating, are observed in the subsequent thermal cycles. The polymers, on the other hand, all show very similar thermal behaviour with a very broad endothermic thermal event occurring with an onset around 50 °C on heating which corresponds to the elimination of the moisture capture during the sample preparation. Subsequent thermal cycles are characterized by a continuous change of the baseline. The thermal stability of the monomers and the polymers was probed by means of thermogravimetric analysis (TGA) at 10 °C min^{-1}. It revealed that all compounds decompose between 260 °C and 280 °C (variations within detection limit) (see Fig. S36–S45).

Using these materials as a host matrix for doping optically active ions, mandates characterization of the optical properties of the neat materials. The UV-Vis transmission spectra of IL monomers and PILs are presented in Fig. 1. The spectra of IL monomers reveal a shoulder in the range of 240–260 nm, which is ascribed to π–π* transitions of the conjugated vinyl double bond. The shoulder is not observed in the spectra of PILs due to the disappearance of the double bond after polymerization. Consequently, all PILs demonstrate high transparency at short wavelengths as well as in the entire visible range, which is mandatory for the desired application. To further characterize the optical properties of the neat PILs, photoluminescence spectra where recorded (Fig. 2). Upon excitation at 315 nm, the PILs display broad band emission with a maximum between 420 and 430 nm. These spectral features are similar to those observed for 1-*n*-alkyl-3-methylimidazolium halides[54]

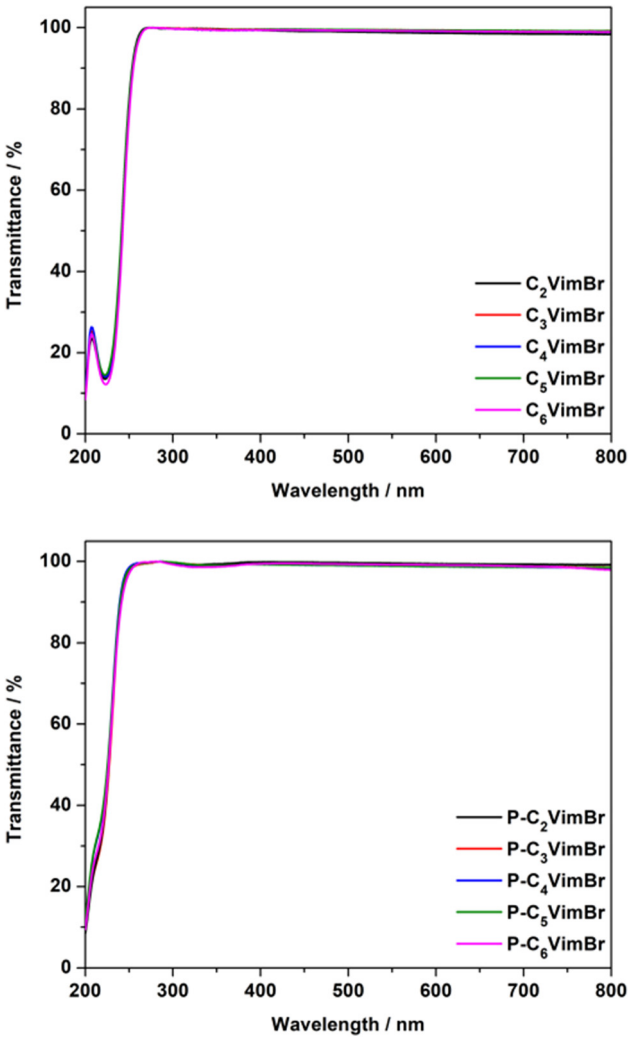

Fig. 1 UV-Vis transmission spectra of IL monomers (top) and PILs (bottom).

and consequently the transition is being identified as the allowed $^{1}\pi^{*} \rightarrow {}^{1}\pi$ transitions of the imidazolium head groups.

The synthesized poly(1-alkyl-3-vinylimidazolium bromides) were then doped with lanthanide(III) halides by combining their anhydrous ethanolic solutions followed by evaporation of ethanol using traditional Schlenk techniques (Scheme 2). Different concentrations of lanthanide(III) halide (1, 5, 10 and 20 mol% with respect to one equivalent of imidazolium in the PIL) were explored to study the influence of the dopant concentration on the emission properties of the final materials.

Additionally, Eu^{3+} can be used as a local structure probe, as its optical properties strongly depend on the local environment[55] and thus, allowing to obtain information about its direct surrounding in the PIL. To determine the impact of the halide ion on the luminescent properties, both chloride and bromide salts of Eu(III) and Tb(III) ion were investigated. The chloride ion is a stronger ligand for lanthanide metals centres compared to the bromide one, rendering them more water stable. However, bromide-containing PILs bear the advantage of easy and clean synthesis.

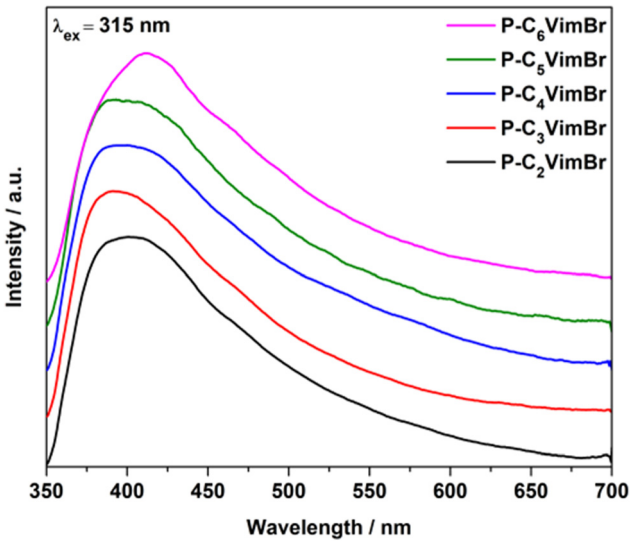

Fig. 2 Emission spectra of PILs collected upon excitation at λ_{ex} = 315 nm.

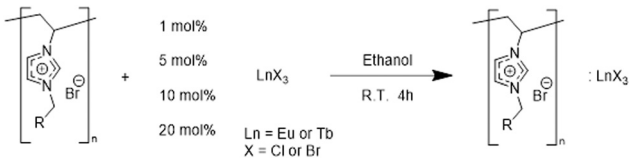

Scheme 2 General procedure for Ln^{3+}-doping of the PILs.

Europium(III) and terbium(III) were chosen because of their reliable emission with good colour purity in red and green. Photoluminescence measurements were performed to investigate the emission properties of the Ln^{3+}-doped PILs. First, steady-state emission spectra were recorded upon excitation at the f–f transition of the respective lanthanide(III) ion, namely the $^{7}F_0 \rightarrow {}^{5}L_6$ transition at 393 nm for the Eu^{3+} ion and the $^{7}F_6 \rightarrow {}^{5}G_6$ transition at 377 nm for the Tb^{3+} ion. Because of great similarity, the spectra of P-C_3VimBr based compounds are shown as representative data in Fig. 3, while the other series are displayed in (Fig. S46–S93). Regardless of the degree of doping, all materials, show the characteristic emission bands caused by the typical f–f transitions of the Eu^{3+} and Tb^{3+} ions. Furthermore, particularly for low dopant concentrations, a broad underlying band with a maximum in the blue-green region of the visible spectrum can be noticed, similarly to the band observed for undoped PILs originating from the $\pi^{*} \rightarrow \pi$ transitions of the imidazolium head groups. This can be confirmed by time-resolved measurements (see Fig. S94). As expected from reports on the luminescence of similar imidazolium based IL compounds,[56] in the spectra recorded with a delay of 0.05 ms, the broad band is no longer visible due to the relatively short lifetimes of the $\pi^{*} \rightarrow \pi$ transitions.[57] For the Eu^{3+}-containing materials, the ratio of the emission intensity of the hypersensitive electric dipole $^{5}D_0 \rightarrow {}^{7}F_2$ transition (610 nm) to the emission intensity of the magnetic dipole $^{5}D_0 \rightarrow {}^{7}F_1$ transition (590 nm) is known as the asymmetry ratio and can be used to analyse the local environment of the lanthanide(III)

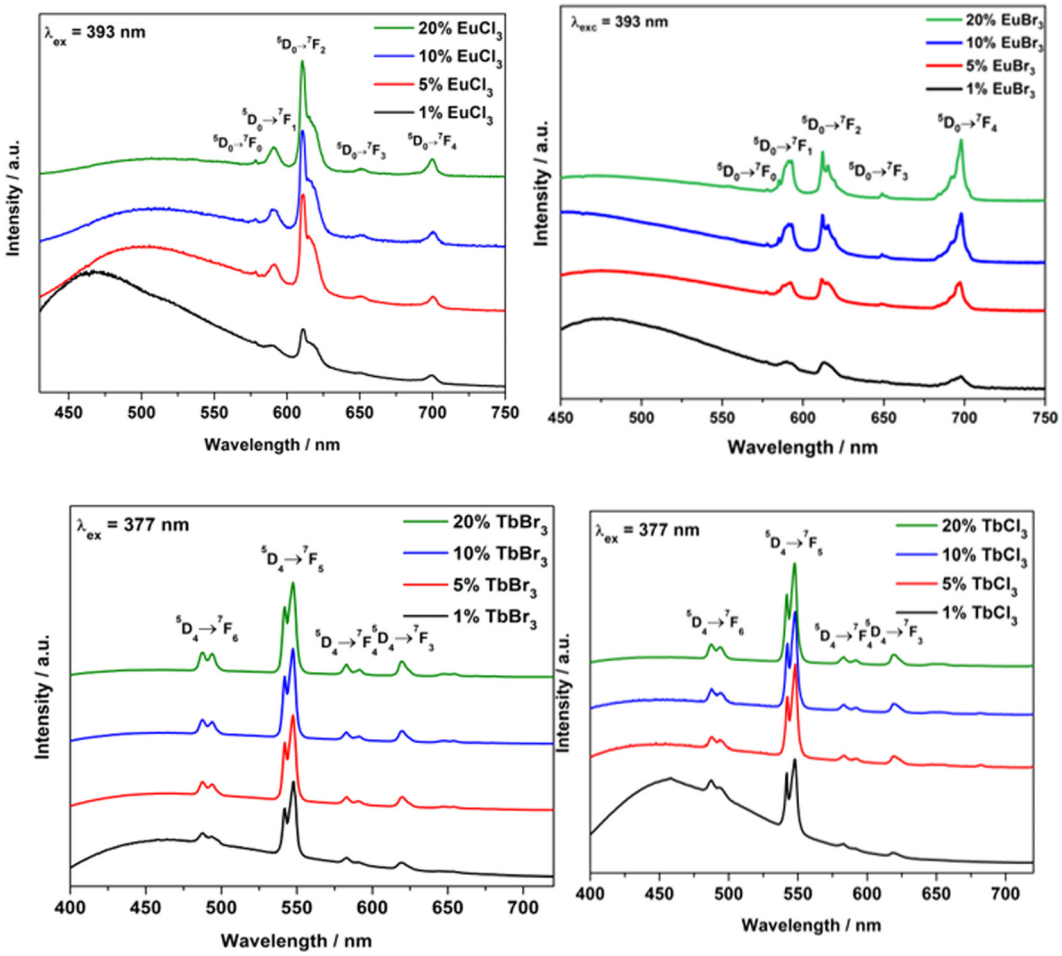

Fig. 3 Emission spectra of P-C_3VimBr doped with different concentrations of $EuCl_3$ (top, left), $EuBr_3$ (top, right), $TbCl_3$ (bottom, left) and $TbBr_3$ (bottom, right).

ion.[58] The emission intensity of the hypersensitive electric dipole transition depends strongly on the site symmetry of the Eu^{3+} ion, while the magnetic dipole transition is insensitive to the environmental changes around the Eu^{3+} ion. Typically, upon reaction of lanthanide(III) halides with organic halides, octahedral hexahalogenido complex anions are obtained.[24,28,29] For $[C_{12}mim]_4[EuBr_6]Br$ a value of 1.26 is reported,[35] similar values are found for $[pyH]_3[EuX_3]$ (pyH = pyridinium, X = Cl, Br).[59] For all PILs doped with $EuBr_3$ an asymmetry ratio close to 1 (1.3 on average) independent of the doping concentrations was found. For the $EuCl_3$-doped PILs, the $[\int(^5D_0 \rightarrow {}^7F_2)/\int(^5D_0 \rightarrow {}^7F_1)]$ asymmetry ratio is higher, and it varies with the doping concentration. Values calculated between 2 (for the lower doping amount) and 4 (for the more concentrated compounds) (Table S1, SI). The fact that the $^5D_0 \rightarrow {}^7F_2$ emission band is much more intense than the $^5D_0 \rightarrow {}^7F_1$ emission band suggests that the Eu^{3+} ion is in a lower symmetry environment. For comparison, in the elpasolite $Cs_2NaEuCl_6$,[60,61] where the Eu^{3+} ion is octahedrally coordinated in a symmetrical distorted environment by chloride ligands, the value equals 1.4. Values higher than 2 have been reported for $[C_{12}mim]Cl$, where Eu^{3+} has been introduced as chloride (2.9), perchlorate (2.9) and triflate (3.2) and nitrate (4.8).[56] As with increasing $EuCl_3$ doping in the bromide-based PIL, the asymmetry ratio increases, it is concluded that at low $EuCl_3$ concentrations upon dissolution bromide is predominately present in the coordination sphere of Eu^{3+}, whilst at high $EuCl_3$ concentration an increasingly mixed halide coordination is occurring. The characteristics of the Eu^{3+} emission profiles do not vary greatly for different concentrations of $EuCl_3$ and $EuBr_3$. However, the higher the dopant concentration, the less intense the emission band from the $\pi^* \rightarrow \pi$ transitions of the imidazolium head groups as compared to the emission bands from the f–f transitions of the Eu^{3+} ion as shown for in P-C_3VimBr in Fig. 3. By comparing the emission spectra of PILs bearing different alkyl chain lengths on cation but featuring the same dopant concentration no distinct changes can be noticed in terms of Eu^{3+} transitions band profile.

The Tb^{3+} ion is known to be an efficient emitter of green light originating from the electronic transitions from the $^5D_4$ excited state to the ^7F_J multiplet of the ground state.[61] The corresponding emission bands are apparent in the collected emission spectra (Fig. 3). Like the Eu^{3+}-doped PILs, the emission spectra of Tb^{3+}-doped PILs demonstrate that the intensity

of the emission bands from f–f transitions increases with increasing dopant concentration, while the intensity of the emission band from the π* → π transitions decreases (Fig. 3). The excitation spectra of Eu^{3+} and Tb^{3+}-doped PILs were recorded by monitoring the most intense $^7F_0 \rightarrow {}^5D_2$ transition at 610 nm for the Eu^{3+} ion and the $^5D_4 \rightarrow {}^7F_5$ transition at 547 nm for the Tb^{3+} ion (Fig. 4). As expected, a series of excitation bands, which can be ascribed to the characteristic f–f transitions of the respective lanthanide(III) ion, is found. In addition, for both Eu^{3+} and Tb^{3+}-doped PILs, a broad band with a maximum at 315 nm, arising from the π → π* transitions of the imidazolium head groups, is observed. The intensity of this excitation band decreases as the dopant concentration increases. For the Tb^{3+}-doped PILs, an additional broad band at 280 nm, which has been reported for the allowed f–d transition ($^7F_6 \rightarrow {}^9D$).[62] A different behaviour was observed for $EuBr_3$-doped polymers. In this case, the imidazolium band was not evident in the excitation spectrum. Moreover, this transition (corresponding to 393 nm) was the dominant one in the excitation spectra of the $EuBr_3$-doped compounds, while the $EuCl_3$-doped series showed a highly intense $^7F_0 \rightarrow {}^5D_2$ transition. The differences in the excitation spectra can be related to a different local symmetry of Eu^{3+} ion and on a different influence of Cl^- and Br^-, as already discussed for the emission spectra.

For both Eu^{3+} and Tb^{3+}-doped PILs, direct excitation into the band at 315 nm gives a noticeably brighter lanthanide(III) emission and better-resolved spectra (Fig. 5). This may suggest that an energy transfer process takes place in doped PILs, whereby energy initially absorbed by the PIL is transferred to the lanthanide(III) ion, which then emits visible light. This process, illustrated in Fig. 6, would explain the apparently much brighter lanthanide(III) emission, as the formally allowed π → π* transitions in the PIL would absorb much more radiation than the parity forbidden f–f transitions. Sensitization of lanthanide(III) ions using organic molecules is widely reported[9,63] and used in different applications such as biolabeling, solar cells, organic electroluminescent devices and LEDs.[64–67] Energy transfer from the imidazolium cation to the lanthanide(III) ion has already been reported for ionic liquid crystals.[56] To further corroborate the energy transfer hypothesis, time-resolved excitation spectra were collected with a delay of 0.05 ms, thereby eliminating any effect from short-lived

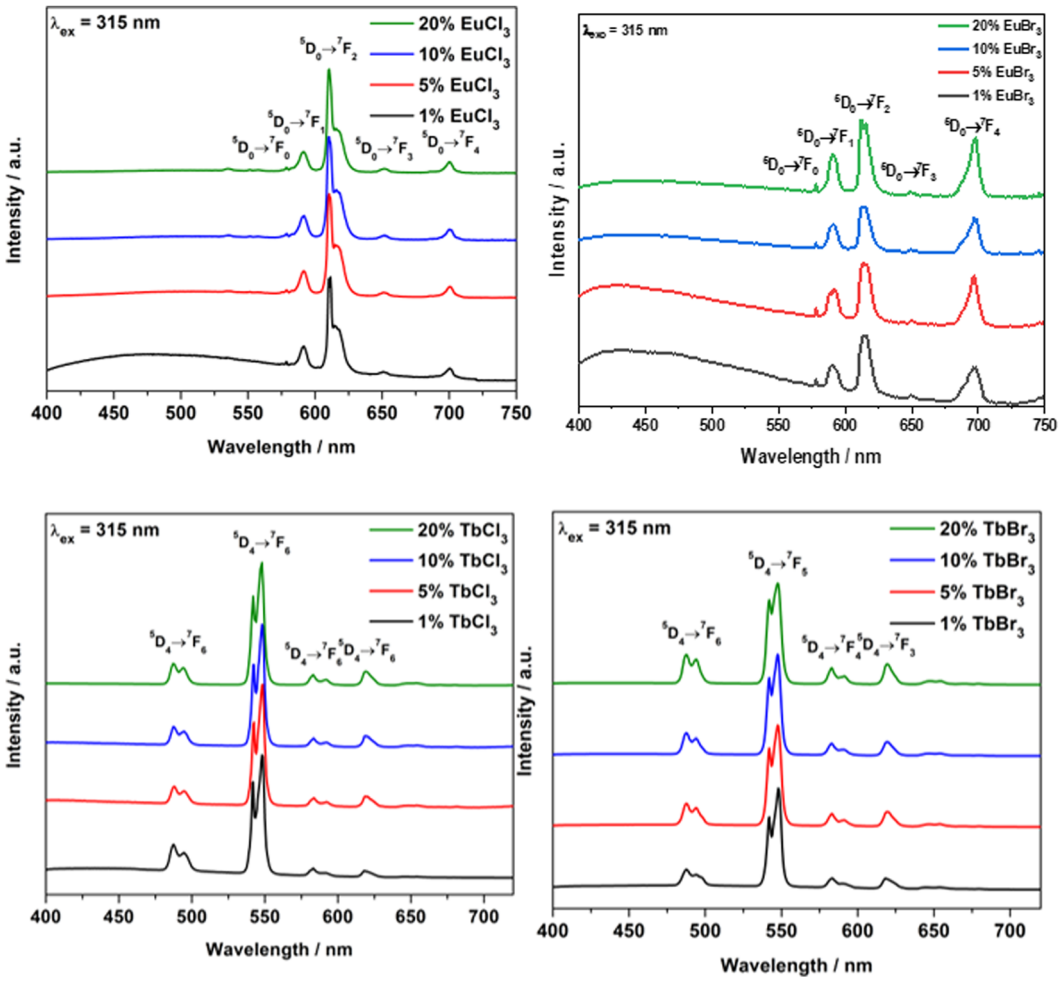

Fig. 4 Excitation spectra of P-C_3VimBr doped with different concentrations of $EuCl_3$ (top, left), $EuBr_3$ (top, right), $TbCl_3$ (bottom, left) and $TbBr_3$ (bottom, right).

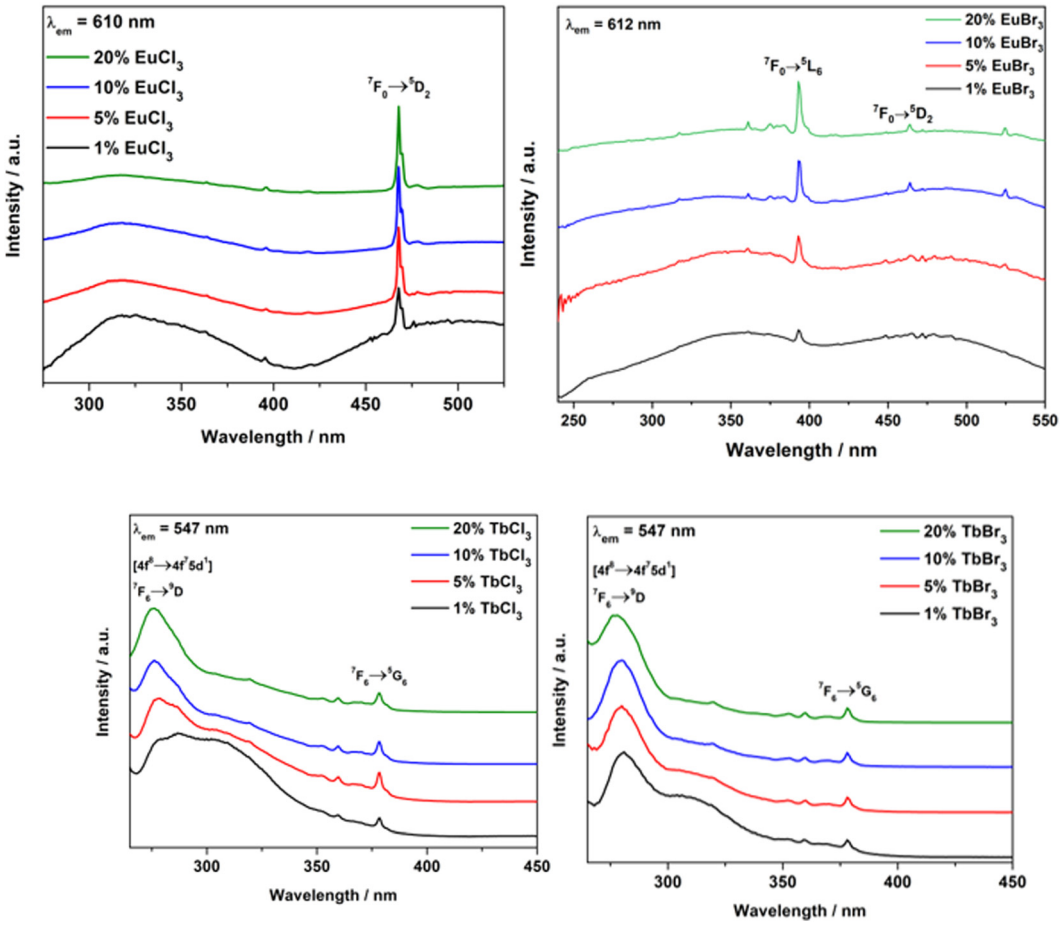

Fig. 5 Emission spectra of P-C_3VimBr doped with different concentrations of $EuCl_3$ (top, left), $EuBr_3$ (top, right), $TbCl_3$ (bottom, left) and $TbBr_3$ (bottom, right).

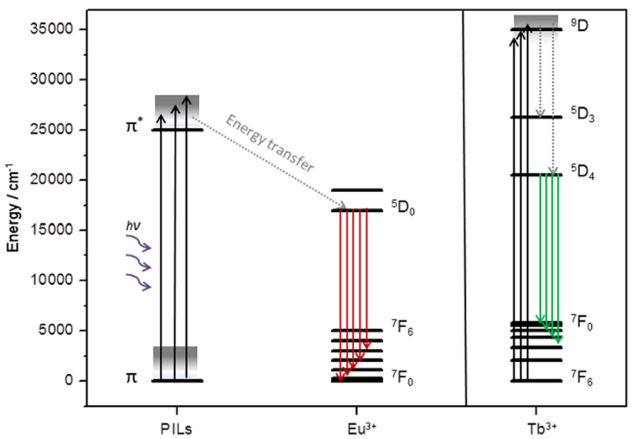

Fig. 6 Energy level diagram illustrating the energy transfer from the PILs to the lanthanide(III) ion.

organic fluorescence (Fig. 7). The broad band located at 315 nm in the steady-state spectrum of the Tb^{3+}-doped P-C_3VimBr, is no longer prominent in the time-resolved spectrum. However, a strong band with a maximum at 280 nm, assigned to the f–d transition, is clearly visible and unperturbed by any signal resulting from the PIL. In contrast, in the time-resolved spectrum of the Eu^{3+}-doped P-C_3VimBr material f–f absorption lines (including VUV absorption lines) are apparent.[68] Although the given resolution is low and does not allow a clear distinction of the VUV f–f absorption lines, the observed broad band may originate from the energy transfer from the PIL to the luminescent Eu^{3+} ion.

Eu^{3+} and Tb^{3+}-doped compounds exhibit an emission colour that is proven to be tuneable by changing the applied excitation wavelength.[37] As the dopant lanthanide(III) ion and the PIL emit light upon photo-excitation, the superposition of both, the dopant and the PIL emission, generates an overall emission with different colour impressions depending on the selected excitation wavelength. CIE-colour coordinates were calculated from the emission spectra obtained by excitation at different wavelengths (Fig. 9 and 10). The respective CIE-colour coordinates demonstrate that the emission colour can be tuned from red (for Eu^{3+}-doped PILs) through green (for Tb^{3+}-doped PILs) to blue (for undoped PILs). In between, several emission colours are realized *via* superposition of the respective lanthanide(III) ion and PIL emission.

Luminescence lifetimes of Eu^{3+} and Tb^{3+}-doped PILs were also determined based on the measurement of decay curves. The obtained decay curves could be best fitted by the sum of

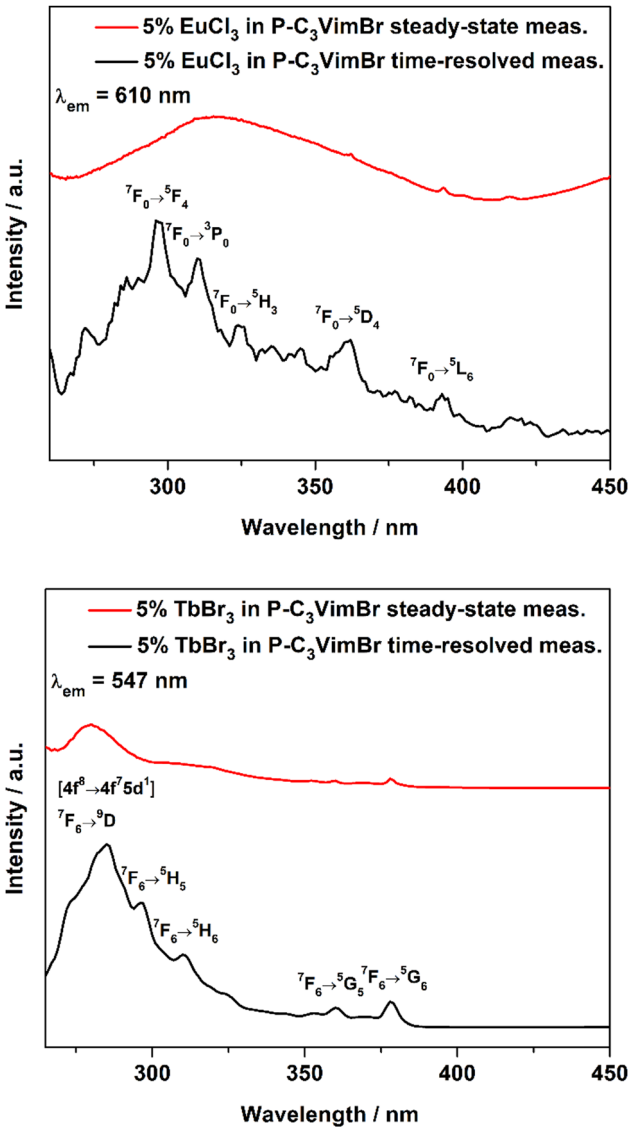

Fig. 7 Time-resolved excitation spectra recorded with a time delay of 0.05 ms *vs.* steady state excitation spectra for 5% $EuCl_3$ in P-C_3VimBr (top) and for 5% $TbBr_3$ in P-C_3VimBr (bottom).

two exponential functions, indicating that the lanthanide(III) ions are in different environments within the same PIL. Average lifetime values, calculated for PILs doped with $EuCl_3$, $EuBr_3$, $TbCl_3$ and $TbBr_3$, are in the range of 0.34–1.06 ms, 0.017–0.131 ms, 1.64–2.42 ms and 1.27–2.02 ms, respectively (see Tables S2–S5 and Fig. S95–S98). It can be noticed that Eu^{3+}-doped PILs possess systematically shorter lifetimes than Tb^{3+}-doped PILs. This is explainable in the view of a smaller energy gap between the lowest excited state and the ground state of Eu^{3+} compared to Tb^{3+}, which makes it easier to go *via* non-radiative vibrational relaxation to the ground state. For the $EuCl_3$-doped PILs, the average lifetime decreases as the dopant concentration increases (see Fig. 8). This phenomenon is often observed in inorganic materials and is known as concentration quenching.[69] However, it has to be kept in mind that from the change in asymmetry ratio a change in the coordination sphere of Eu^{3+} occurs, which also

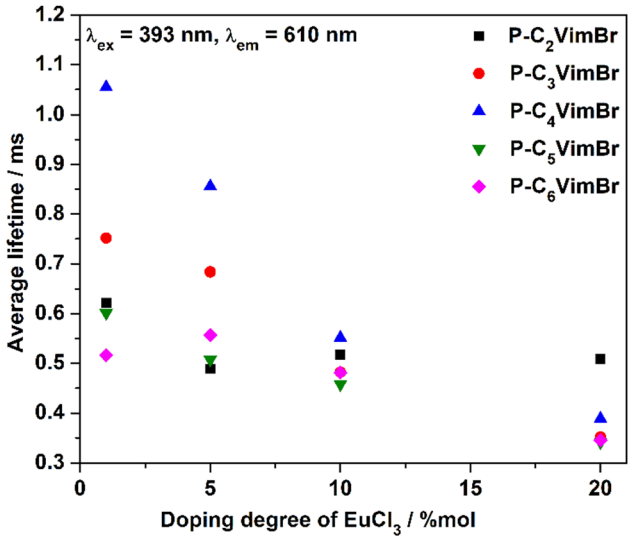

Fig. 8 Lifetimes of PILs doped with different concentrations of $EuCl_3$.

impacts the lifetime. Interestingly, in the case of $EuBr_3$-doped materials, no correlation between lifetime and dopant concentration was found. Moreover, the series show a distinct, but not clearly systematic dependence on the cation of the alkyl chain length. This can be explained by two opposing effects: by varying the chain length, the lanthanide(III)–lanthanide(III) distance also change, which on the one hand would reduce the likelihood of concentration quenching. On the other, the probability of a vibrational quenching increases due to the presence of more C–H bonds. It is worth noting that the lifetimes for PILs doped with $TbCl_3$ are on average longer than those for PILs doped with $TbBr_3$.

Experimental

Materials

1-Bromoethane (99%), 1-bromopropane (99%), 1-bromobutane (99%), 1-bromopentane (99%), 1-bromohexane (99%) and azo-bis(isobutyronitrile) (AIBN) (98%) were purchased from Sigma-Aldrich (Steinheim, Germany) and used as received. 1-Vinylimidazole (98%) was purchased from Alfa Aesar (Kandel, Germany) and distilled under reduced pressure prior to use. Tb_4O_7 (99.99%) was purchased from HEFA Rare Earth Canada Co. Ltd (Richmond, British Columbia, Canada). $EuCl_3$ (anhydrous, 99.9%) and HBr (48%) were purchased from abcr (Karlsruhe, Germany). HCl (37%), HBr (48%), NH_4Cl, NH_4Br and anhydrous ethanol (99.5%) were purchased from Acros Organic (Geel, Belgium). 1-Vinylimidazole was distilled over KOH before use. The other chemicals were used as received.

Instrumentation

^{1}H- and ^{13}C-NMR spectra were acquired on DMSO-d_6 solutions using a Bruker 400 MHz spectrometer equipped with a BBO probe (Bruker AXS, Karlsruhe, Germany). Chemical shifts are reported in delta (δ) units, expressed in parts per million (ppm). The following abbreviations were used for the observed

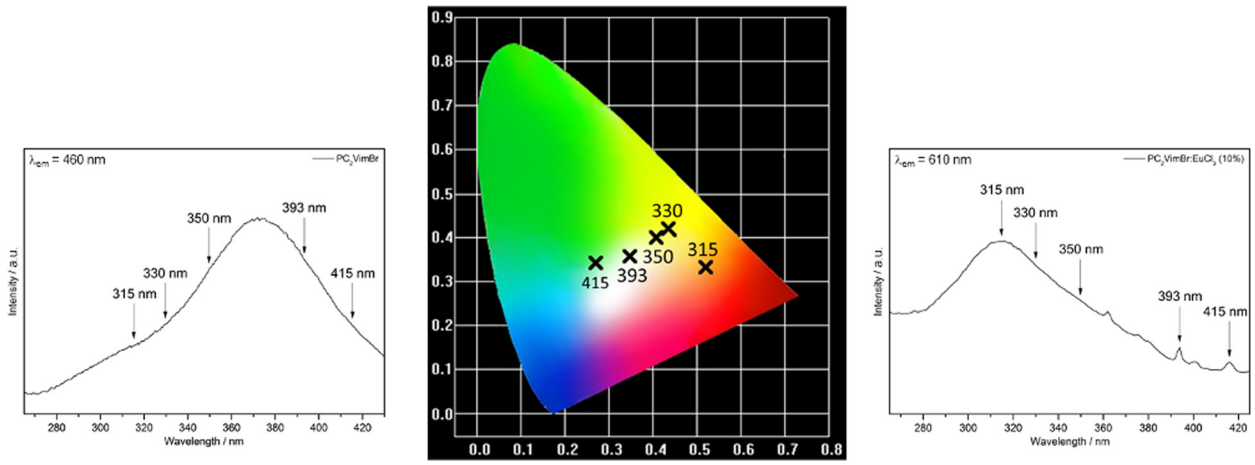

Fig. 9 Representative calculated colour coordinates for 10% $EuCl_3$ in P-C_3VimBr at different excitation wavelengths.

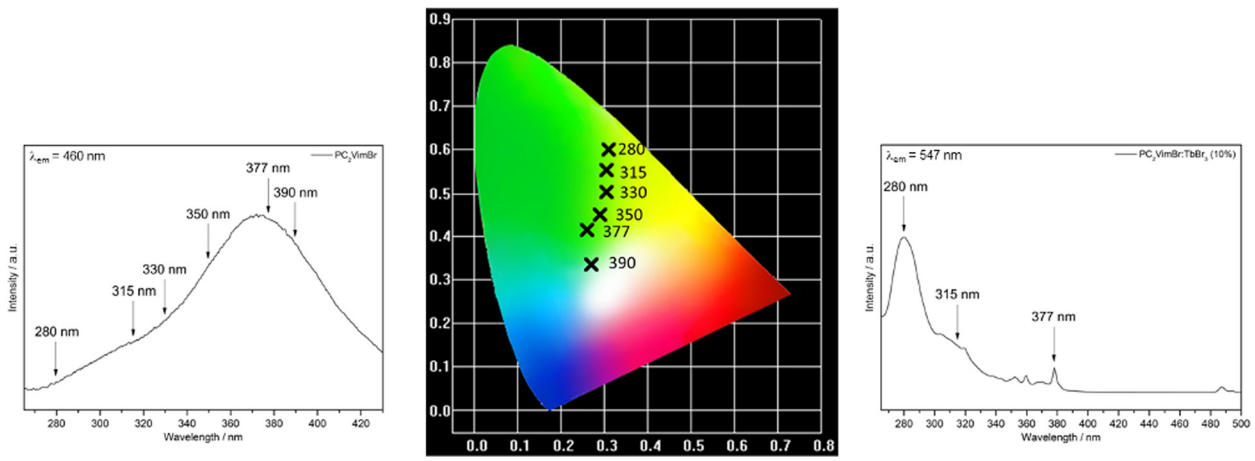

Fig. 10 Representative calculated colour coordinates for 10% $TbBr_3$ in P-C_3VimBr at different excitation wavelengths.

multiplicities: s (singlet), d (doublet), t (triplet), q (quartet), p (pentuplet), h (hexuplet), bs (broad singlet), dd (double doublet) m (multiplet for unresolved lines). ^{1}H-NMR chemical shifts were referenced to the residual solvent signal for DMSO (2.50 ppm) and ^{13}C-NMR chemical shifts were referenced to the solvent signal of DMSO (39.52 ppm).

Fourier transform infrared spectra (FTIR) were collected on a Bruker Alpha-P ATR-spectrometer equipped with a diamond crystal (Bruker, Ettlingen, Germany) in attenuated total reflection configuration. The data evaluation was carried out with the program OPUS (Bruker, Ettlingen, Germany).

UV-vis absorption spectra were recorded on ethanol solutions with an Agilent Technologies Cary 5000 UV-vis-NIR spectrophotometer (Santa Clara, CA, USA) using 1 cm light-path quartz cuvettes.

Photoluminescence measurements were carried out on a Horiba Jobin Yvon Fluorolog FL 3–22 spectrofluorometer (Horiba JobinYvon, Longjumeau, France). In steady-state measurements, a continuous xenon lamp (450 W) and an R928P PMT detector were used for sample excitation and signal detection, respectively. In time-resolved measurements, sample excitation was realized with a pulsed xenon lamp.

Thermogravimetric Analyses (TGA) were performed with a TG 449 F3 Jupiter (Netzsch, Selb, Germany). Measurements were carried out in aluminum oxide crucibles with a heating rate of 10 °C min^{-1} and nitrogen as purge gas with a flow rate of 40 mL min^{-1}. Given temperatures correspond to a 5% onset with a standard deviation of ±1 °C.

Differential scanning calorimetry (DSC) was performed with a computer-controlled PhoenixDSC 204 F1 thermal analyzer (Netzsch, Selb, Germany). A heating rate of 5 °C min^{-1} was used for the measurements that are carried from −60 °C to 150 °C under an argon atmosphere supplied by a flow at a rate of 40 mL min^{-1}. Cold-sealed and punctured aluminium pans were used as sample containers. The samples were first cooled to −60 °C. Given temperatures correspond to the onset of the respective thermal process with a standard deviation of ±0.5 °C. Stated temperatures of glass transition correspond to the midpoint with a standard deviation of ±1 °C.

Powder X-ray diffraction (PXRD) data were recorded at ambient temperature on a PANalytical X'pert PRO diffractometer (Malvern Panalytical, Malvern, United Kingdom), operating at 45 kV and 40 mA and using CuKα1 radiation. The data was

recorded in reflection mode from 5° to 70° with a step size of 0.01° for 60 min with 0.55 s per step. The samples were prepared by dispersing a ground powder on a zero-background silicon wafer.

Synthetic procedures

General procedure for synthesis of ionic liquid monomers. In a Schlenk flask was added 1-vinylimidazole (50 mmol, 1.0 eq.) and the respective alkyl bromide (60 mmol, 1.2 eq.). The solution was then heated at 80 °C during 48 h. After cooling to room temperature, the volatile sub-products were removed under reduced pressure. All the ionic liquids were washed with ethyl acetate (3 × 30 mL) and then dried under dynamic vacuum for 24 h.

1-Ethyl-3-vinylimidazolium bromide C_2VimBr. White powder. ^{1}H-NMR (400 MHz, DMSO-d_6): 1.44 (t, J_{H-H} = 7.3 Hz, 3H), 4.26 (q, J_{H-H} = 7.3 Hz, 2H), 5.40 (dd, J_{H-H} = 8.4 Hz, J_{H-H} = 2.3 Hz, 1H), 6.03 (dd, J_{H-H} = 15.6 Hz, J_{H-H} = 2.4 Hz, 1H), 7.36 (dd, J_{H-H} = 15.7 Hz, J_{H-H} = 8.8 Hz, 1H), 8.04 (t, J_{H-H} = 1.9 Hz, 1H), 8.30 (t, J_{H-H} = 1.9 Hz, 1H), 9.80 (t, J_{H-H} = 1.6 Hz, 1H). ^{13}C-NMR (101 MHz, DMSO-d_6): 14.8, 44.6, 108.6, 119.1, 122.9, 128.8, 135.0. ν_{max} (cm^{-1}): 3131, 3055, 2989, 1660, 1581, 1544, 1458, 1417, 1376, 1345, 1330, 1302, 1258, 1185, 1167, 1136, 1048, 1032, 1010, 978, 926, 888, 854, 782, 715, 690, 634, 618, 595, 486. T_{melt} = 64.3 °C. T_d = 276 °C.

1-Propyl-3-vinylimidazolium bromide C_3VimBr. Colourless oil. ^{1}H-NMR (400 MHz, DMSO-d_6): 0.78 (t, J_{H-H} = 7.4 Hz, 3H), 1.81 (h, J_{H-H} = 7.3 Hz, 2H), 4.22 (t, J_{H-H} = 7.2 Hz, 2H), 5.37 (dd, J_{H-H} = 8.8 Hz, J_{H-H} = 2.5 Hz, 1H), 6.07 (d, J_{H-H} = 15.7 Hz, J_{H-H} = 2.5 Hz, 1H), 7.38 (dd, J_{H-H} = 15.7 Hz, J_{H-H} = 8.8 Hz, 1H), 8.09 (t, J_{H-H} = 1.7 Hz, 1H), 8.39 (t, J_{H-H} = 1.9 Hz, 1H), 9.94 (s, 1H). ^{13}C-NMR (101 MHz, DMSO-d_6): 10.3, 22.6, 50.5, 108.7, 119.2, 123.2, 128.6, 135.1. ν_{max} (cm^{-1}): 3413, 3124, 3053, 2965, 2877, 2726, 1650, 1570, 1548, 1494, 1456, 1414, 1371, 1347, 1311, 1272, 1229, 1170, 1115, 1088, 1046, 1007, 960, 915, 862, 834, 800, 754, 682, 649, 621, 597, 464. T_g = −40 °C. T_d = 277 °C.

1-Butyl-3-vinylimidazolium bromide C_4VimBr. White powder. ^{1}H-NMR (400 MHz, DMSO-d_6): 0.89 (t, J_{H-H} = 7.4 Hz, 3H), 1.28 (h, J_{H-H} = 7.4 Hz, 2H), 1.81 (p, J_{H-H} = 7.5 Hz, 2H), 4.23 (t, J_{H-H} = 7.2 Hz, 2H), 5.41 (dd, J_{H-H} = 8.7 Hz, J_{H-H} = 2.4 Hz, 1H), 6.01 (dd, J_{H-H} = 15.7 Hz, J_{H-H} = 2.4 Hz, 1H), 7.34 (dd, J_{H-H} = 15.6 Hz, J_{H-H} = 8.7 Hz, 1H), 8.00 (t, J_{H-H} = 1.9 Hz, 1H), 8.27 (t, J_{H-H} = 2.0 Hz, 1H), 9.72 (s, 1H). ^{13}C-NMR (101 MHz, DMSO-d_6): 13.3, 18.8, 31.0, 48.9, 108.6, 119.2, 123.2, 128.8, 135.3. ν_{max} (cm^{-1}): 3108, 3091, 3040, 2981, 2968, 2954, 2928, 2872, 2847, 1818, 1758, 1706, 1652, 1566, 1540, 1466, 1458, 1433, 1414, 1366, 1339, 1321, 1291, 1273, 1159, 1115, 1049, 1006, 983, 926, 881, 805, 739, 723, 681, 661, 636, 604, 510, 434. T_{melt} = 81.6 °C. T_d = 264 °C.

1-Pentyl-3-vinylimidazolium bromide C_5VimBr. White powder. ^{1}H-NMR (400 MHz, DMSO-d_6): 0.81 (t, J_{H-H} = 7.1 Hz, 3H), 1.15-1.33 (m, 4H), 1.82 (p, J_{H-H} = 7.3 Hz, 2H), 4.25 (t, J_{H-H} = 7.3 Hz, 2H), 5.39 (dd, J_{H-H} = 8.8 Hz, J_{H-H} = 2.4 Hz, 1H), 6.06 (dd, J_{H-H} = 15.6 Hz, J_{H-H} = 2.4 Hz, 1H), 7.39 (dd, J_{H-H} = 15.7 Hz, J_{H-H} = 8.8 Hz, 1H), 8.08 (t, J_{H-H} = 1.8 Hz, 1H), 8.37 (t, J_{H-H} = 1.9 Hz, 1H), 9.92 (s, 1H). ^{13}C-NMR (101 MHz, DMSO-d_6): 13.6, 21.4, 27.5, 28.8, 49.0, 108.6, 119.2, 123.2, 128.7, 135.2. ν_{max} (cm^{-1}): 3433, 3122, 3040, 2960, 2929, 2858, 1767, 1650, 1571, 1548, 1458, 1415, 1373, 1318, 1276, 1232, 1197, 1166, 1116, 1039, 1010, 963, 923, 868, 787, 750, 734, 694, 650, 620, 599, 488. T_{melt} = 51.8 °C. T_d = 262 °C.

1-Hexyl-3-vinylimidazolium bromide C_6VimBr. Colourless oil. ^{1}H-NMR (400 MHz, DMSO-d_6): 0.81 (t, J_{H-H} = 7.2 Hz, 3H), 1.22 (s, 6H), 1.77–1.85 (m, 2H), 4.25 (t, J_{H-H} = 7.3 Hz, 2H), 5.39 (dd, J_{H-H} = 8.4 Hz, J_{H-H} = 2.4 Hz 1H), 6.06 (dd, J_{H-H} = 15.6 Hz, J_{H-H} = 2.4 Hz 1H), 7.39 (dd, J_{H-H} = 15.7 Hz, J_{H-H} = 8.8 Hz, 1H), 8.07 (t, J_{H-H} = 1.8 Hz, 1H), 8.36 (t, J_{H-H} = 1.9 Hz, 1H), 9.91 (s, 1H). ^{13}C-NMR (101 MHz, DMSO-d_6): 13.7, 21.8, 25.1, 29.0, 30.4, 49.1, 108.5, 119.2, 123.2, 128.7, 135.2. ν_{max} (cm^{-1}): 3416, 3052, 2955, 2929, 2858, 1651, 1570, 1548, 1458, 1414, 1338, 1315, 1273, 1168, 1119, 1084, 1006, 963, 917, 764, 730, 651, 622, 598, 477, 464. T_g = −35 °C. T_d = 264 °C.

General procedure for synthesis for polymerization of ionic liquid monomers. The polymerization of 1-alkyl-3-methylvinylimidazolium followed a modified literature procedure.[47] In a typical polymerization reaction, the respective monomer (5 mmol) was dissolved in chloroform (30 mL). AIBN (azo-bis(isobutyro)nitrile) (2 mol%) was added and the reaction mixture refluxed at 80 °C for 48 h. Then the solvent was evaporated under reduced pressure, and the remaining transparent polymers were dried under dynamic vacuum.

Poly(1-ethyl-3-vinylimidazolium bromide) P-C_2VimBr. Colourless solid. ^{1}H-NMR (400 MHz, DMSO-d_6): 1.38–1.52 (m, 3H), 2.33–2.67 (m, 2H), 4.13–4.64 (m, 3H), 7.65–8.06 (m, 2H), 9.48 (bs, 1H). ν_{max} (cm^{-1}): 3408, 3124, 3045, 2963, 2937, 1741, 1661, 1661, 1661, 1661, 1569, 1548, 1446, 1385, 1338, 1308, 1260, 1160, 1093, 1020, 961, 861, 799, 743, 647, 620, 478, 458, 444, 433. T_d = 264 °C.

Poly(1-propyl-3-vinylimidazolium bromide) P-C_3VimBr. Colourless solid. ^{1}H-NMR (400 MHz, DMSO-d_6): 0.92 (bs, 3H), 1.89 (s, 2H), 2.50 (bs (2H)), 4.10 (bs, 3H), 7.73–8.97 (m, 2H), 9.75 (bs, 1H). ν_{max} (cm^{-1}): 3406, 3121, 3049, 2964, 2934, 2876, 2446, 1637, 1568, 1548, 1455, 1435, 1384, 1368, 1345, 1310, 1261, 1160, 1110, 1020, 904, 864, 800, 741, 648, 621, 505, 467. T_d = 268 °C.

Poly(1-butyl-3-vinylimidazolium bromide) P-C_4VimBr. Colourless solid. ^{1}H-NMR (400 MHz, DMSO-d_6): 0.94 (bs, 3H), 1.33 (bs, 2H), 1.87 (bs, 4H), 2.50 (bs (2H)), 4.14 (bs, 3H), 7.89 (bs, 2H), 9.75 (bs, 1H). ν_{max} (cm^{-1}): 3405, 3125, 3056, 2960, 2933, 2872, 1627, 1568, 1549, 1460, 1436, 1378, 1314, 1261, 1159, 1112, 1025, 949, 800, 746, 648, 622, 557, 537, 488, 472, 455, 403. T_d = 266 °C.

Poly(1-pentyl-3-vinylimidazolium bromide) P-C_5VimBr. Colourless solid. ^{1}H-NMR (400 MHz, DMSO-d_6): 0.92 (bs, 3H), 1.34 (bs, 4H), 1.90 (bs, 4H), 2.50 (bs (2H)), 4.13 (bs, 3H), 7.70–7.90 (m, 2H), 9.79 (bs, 1H). ν_{max} (cm^{-1}): 3413, 3122, 3051, 2956, 2929,

2861, 1629, 1568, 1549, 1457, 1378, 1311, 1262, 1160, 1112, 1022, 930, 857, 798, 744, 648, 621, 532, 493, 453, 429, 411. T_d = 262 °C.

Poly(1-hexyl-3-vinylimidazolium bromide) P-C_6VimBr. Colourless solid. ^{1}H-NMR (400 MHz, DMSO-d_6): 0.89 (bs, 3H), 1.32 (bs, 6H), 1.88 (bs, 4H), 2.50 (bs (2H)), 4.13 (bs, 3H), 7.67–8.09 (m, 2H), 9.78 (bs, 1H). ν_{max} (cm^{-1}): 3407, 3125, 3053, 2955, 2927, 2857, 1626, 1569, 1549, 1457, 1377, 1311, 1262, 1231, 1160, 1113, 1024, 866, 819, 749, 647, 621, 526, 508, 461, 445, 422, 408. T_d = 273 °C.

General procedure for synthesis of terbium halides. For the preparation of terbium halides, the ammonium halide route[70] was employed. In a typical reaction, Tb_4O_7 was dissolved in the respective mineral acid (HCl/HBr) by heating to 100 °C. A minimum 12-fold excess of ammonium halide was added to the resulting solution. The water and acid were boiled off, until an almost dry, pale-yellow solid remained. The decomposition of the respective ammonium hexahalogenoterbate was achieved by heating to 450 °C under dynamic vacuum for 24 h. For further purification, terbium chloride was sublimed at 700 °C under 10^{-6} mbar. The purity of terbium halides was checked by PXRD.

General procedure for preparation of the luminescent organic–inorganic hybrid materials. The main paragraph text follows directly on here. The respective polymer (100 mg) was dissolved in ethanol (10 mL) under vigorous stirring. The lanthanide halide to be used was either dissolved or dispersed in ethanol (10 mL). Following this, the homogeneous polymer solution was split into four fractions (each of 2.5 mL). Each fraction was then charged with the required volume of lanthanide halide solution or dispersion to produce a lanthanide halide dopant concentration of 1, 5, 10 and 20 mol% with respect to one imidazolium equivalent in the polymer. After two hours of intense stirring at room temperature, the solvent was removed, and the samples were dried under dynamic vacuum for 48 h.

Conclusions

A simple route to luminescent organic–inorganic hybrid materials has been established by dispersing lanthanide(III) halides in ionic liquid polymers based on 1-alkyl-3-vinylimidazolium bromides. The resulting materials could be chemically described as poly(1-alkyl-3-vinylimidazolium) cations with a mixture of halide (X^-) and halogenolanthanidate ($[Ln_xX_y]^{3x-y}$) counterions. Photoluminescence measurements have shown that energy transfer from the polymer itself to the dopant ion is possible, leading to enhanced emission. Furthermore, the prepared materials demonstrate tuneable colour emission ranging from deep red (for Eu^{3+}-doped PILs) through green (for Tb^{3+}-doped PILs) to blue (for undoped PILs) by altering the excitation wavelength. This indicates a high potential of these materials for applications.

Conflicts of interest

There are no conflicts to declare.

Data availability

Supplementary information: The content of the Supplementary information is data on synthesis, materials characterization and purity (NMR, IR), thermal behaviour (TG, DSC) and optical properties (absorption, excitation and emission spectra). See DOI: https://doi.org/10.1039/d5ma00282f

Acknowledgements

The Novonordisk Foundation is acknowledged for research support of the SMARTER – Salt Melts for Advanced Reactor Technology and Energy Research. AVM would like to thank the Carl Tryggers Foundation (Stockholm, Sweden) for a fellowship for MWK. AVM acknowledges VR for support through project no. 2020-04437. Demian Pitz is acknowledged for initial experimental work together with support from the DFG Cluster of excellence, RESOLV.

References

1 A. E. Outlook, US Energy Information Administration: Washington, DC, USA, 2019.
2 E. F. Schubert, *Light-emitting diodes*, 2006, p. 1.
3 Z. Koretsky, *Energy Res. Soc. Sci.*, 2021, **82**, 102310.
4 W. Gao, Z. Sun, Y. Wu, J. Song, T. Tao, F. Chen, Y. Zhang and H. Cao, *Clean. Eng. Technol.*, 2022, **6**, 100380.
5 B. Adranno, S. Tang, V. Paterlini, V. Smetana, O. Renier, G. Bousrez, L. Edman and A.-V. Mudring, *Adv. Photo. Res.*, 2023, **4**, 2200351.
6 S. Li, L. Zhou and H. Zhang, *Light: Sci. Appl.*, 2022, **11**, 177.
7 V. V. Utochnikova, in *Handbook on the Physics and Chemistry of Rare Earths*, ed. J.-C. G. Bünzli and V. K. Pecharsky, Elsevier, 2021, vol. 59, p. 1.
8 D. A. Chengelis, A. M. Yingling, P. D. Badger, C. M. Shade and S. Petoud, *J. Am. Chem. Soc.*, 2005, **127**, 16752.
9 P. Mukherjee, C. M. Shade, A. M. Yingling, D. N. Lamont, D. H. Waldeck and S. Petoud, *J. Phys. Chem. A*, 2011, **115**, 4031.
10 S. Viswanathan and A. de Bettencourt-Dias, *Inorg. Chem.*, 2006, **45**, 10138.
11 D. Prodius, K. Gandha, A.-V. Mudring and I. C. Nlebedim, *ACS Sustainable Chem. Eng.*, 2020, **8**, 1455.
12 K. Binnemans, *Chem. Rev.*, 2009, **109**, 4283.
13 E. H. Huffman, *Phys. Lett.*, 1963, **7**, 237.
14 E. H. Huffman, *Nature*, 1963, **200**, 158.
15 D. Wang, J. Zhang, Q. Lin, L. Fu, H. Zhang and B. Yang, *J. Mater. Chem.*, 2003, **13**, 2279.
16 J. Yuan and M. Antonietti, *Polymer*, 2011, **52**, 1469.
17 J. Yuan, D. Mecerreyes and M. Antonietti, *Prog. Polym. Sci.*, 2013, **38**, 1009.
18 D. Mecerreyes, *Prog. Polym. Sci.*, 2011, **36**, 1629.
19 J. Lu, F. Yan and J. Texter, *Prog. Polym. Sci.*, 2009, **34**, 431.
20 M. D. Green and T. E. Long, *Polym. Rev.*, 2009, **49**, 291.
21 O. Green, S. Grubjesic, S. Lee and M. A. Firestone, *Polym. Rev.*, 2009, **49**, 339.

22 W. Xiao, Q. Yang and S. Zhu, *Sci. Rep.*, 2020, **10**, 7825.
23 B. Mallick, B. Balke, C. Felser and A.-V. Mudring, *Angew. Chem., Int. Ed.*, 2008, **47**, 7635.
24 A. Babai and A.-V. Mudring, *Chem. Mater.*, 2005, **17**, 6230.
25 S. Tang, A. Babai and A.-V. Mudring, *Angew. Chem., Int. Ed.*, 2008, **47**, 7631.
26 S. Arenz, A. Babai, K. Binnemans, K. Driesen, R. Giernoth, A.-V. Mudring and P. Nockemann, *Chem. Phys. Lett.*, 2005, **402**, 75.
27 A. Babai and A.-V. Mudring, *Inorg. Chem.*, 2005, **44**, 8168.
28 A. Babai and A.-V. Mudring, *J. Alloys Compd.*, 2006, **418**, 122.
29 A.-V. Mudring, A. Babai, S. Arenz, R. Giernoth, K. Binnemans, K. Driesen and P. Nockemann, *J. Alloys Compd.*, 2006, **418**, 204.
30 A. Getsis, B. Balke, C. Felser and A.-V. Mudring, *Cryst. Growth Des.*, 2009, **9**, 4429.
31 S. F. Tang and A. V. Mudring, *Eur. J. Inorg. Chem.*, 2009, 2769.
32 S. Tang, J. Cybińska and A.-V. Mudring, *Helv. Chim. Acta*, 2009, **92**, 2375.
33 B. Kirchner, *Ionic liquids from theoretical investigations*, Springer, 2010.
34 A.-V. Mudring and S. Tang, *Eur. J. Inorg. Chem.*, 2010, 2569.
35 A. Getsis, S. Tang and A.-V. Mudring, *Eur. J. Inorg. Chem.*, 2010, 2172.
36 A. Getsis and A.-V. Mudring, *Z. Anorg. Allg. Chem.*, 2010, **636**, 1726.
37 A. Getsis and A.-V. Mudring, *Eur. J. Inorg. Chem.*, 2011, 3207.
38 Q. Ju, P. S. Campbell and A.-V. Mudring, *J. Mater. Chem. B*, 2013, **1**, 179.
39 Q. Ju and A. V. Mudring, *RSC Adv.*, 2013, **3**, 8172–8175.
40 P. Ghosh, S. Tang and A.-V. Mudring, *J. Mater. Chem.*, 2011, **21**, 8640.
41 J. Cybińska, C. Lorbeer, E. Zych and A. V. Mudring, *ChemSusChem*, 2011, **4**, 595.
42 C. Lorbeer, J. Cybińska and A.-V. Mudring, *Cryst. Growth Des.*, 2011, **11**, 1040.
43 A.-V. Mudring, J. Nuss, U. Wedig and M. Jansen, *J. Solid State Chem.*, 2000, **155**, 29.
44 P. Ghosh, C. Lorbeer and A.-V. Mudring, *Fluorine-Related Nanoscience with Energy Applications*, American Chemical Society, 2011, vol. 1064, p. 87.
45 C. Lorbeer and A.-V. Mudring, *J. Phys. Chem. C*, 2013, **117**, 12229.
46 C. Lorbeer, J. Cybińska and A.-V. Mudring, *J. Mater. Chem. C*, 2014, **2**, 1862.
47 P. S. Campbell, C. Lorbeer, J. Cybińska and A.-V. Mudring, *Adv. Funct. Mater.*, 2013, **23**, 2924.
48 R. Marcilla, J. Alberto Blazquez, J. Rodriguez, J. A. Pomposo and D. Mecerreyes, *J. Polym. Sci., Part A: Polym. Chem.*, 2004, **42**, 208–212.
49 M. D. Green, D. Salas-de la Cruz, Y. Ye, J. M. Layman, Y. A. Elabd, K. I. Winey and T. E. Long, *Macromol. Chem. Phys.*, 2011, **212**, 2522.
50 J. C. Salamone, S. Israel, P. Taylor and B. Snider, *Polymer*, 1973, **14**, 639.
51 *A Practical Guide to Understanding the NMR of Polymers*, ed. P. A. Mirau, Wiley-Interscience, 2005.
52 J. Pinaud, J. Vignolle, Y. Gnanou and D. Taton, *Macromolecules*, 2011, **44**, 1900–1908.
53 *Infrared and Raman characteristic group frequencies: tables and charts*, ed. G. Socrates, John Wiley & Sons, 2004.
54 A. Getsis and A.-V. Mudring, *Cryst. Res. Technol.*, 2008, **43**, 1187.
55 *Phosphor Handbook*, ed. W. M. Yen, S. Shionoya and H. Yamamoto, The CRC Press laser and optical science and technology series, CRC Press/Taylor and Francis, Boca Raton, FL, 2nd edn, 2007.
56 E. Guillet, D. Imbert, R. Scopelliti and J.-C. G. Bünzli, *Chem. Mater.*, 2004, **16**, 4063.
57 *Molecular fluorescence: principles and applications*, ed. B. Valeur and M. N. Berberan-Santos, John Wiley & Sons, 2013.
58 *Handbook on the physics and chemistry of rare earths*, ed. L. Eyring, K. A. Gschneidner and G. Lander, Elsevier, 2002.
59 E. Butter, *Z. Anorg. Allg. Chem.*, 1968, **356**, 294.
60 L. R. Morss, M. Siegal, L. Stenger and N. Edelstein, *Inorg. Chem.*, 1970, **9**, 1771.
61 C. Klixbüll Jørgensen, *Prog. Inorg. Chem.*, 1970, 101.
62 A. Srivastava, H. Comanzo, S. Camardello, M. Aycibin and U. Happek, *Opt. Mater.*, 2012, **34**, 591.
63 F. Pointillart, T. Cauchy, O. Maury, Y. Le Gal, S. Golhen, O. Cador and L. Ouahab, *Chem. – Eur. J.*, 2010, **16**, 11926.
64 S.-S. Zhou, X. Xue, J.-F. Wang, Y. Dong, B. Jiang, D. Wei, M.-L. Wan and Y. Jia, *J. Mater. Chem.*, 2012, **22**, 22774.
65 K. Kawano, K. Arai, H. Yamada, N. Hashimoto and R. Nakata, *Sol. Energy Mater. Sol. Cells*, 1997, **48**, 35.
66 S. Dirr, H.-H. Johannes and W. Kowalsky, *Annu. Rep.*, 1995, 64–68.
67 M. Koppe, H. Neugebauer and N. S. Sariciftci, *Mol. Cryst. Liq. Cryst.*, 2002, **385**, 101.
68 Y.-C. Li, Y.-H. Chang, Y.-F. Lin, Y.-S. Chang and Y.-J. Lin, *J. Alloys Compd.*, 2007, **439**, 367–375.
69 D. L. Dexter and J. H. Schulman, *J. Chem. Phys.*, 1954, **22**, 1063.
70 H. H. Anderson, *J. Am. Chem. Soc.*, 1961, **83**, 505.